Research Article

Noura El-Ahmady El-Naggar, Ragaa A. Hamouda*, Muhammad A. Abuelmagd, Maha M. Alharbi, Doaa Bahaa Eldin Darwish, Nashwa H. Rabei, and Safinaz A. Farfour

A cost-effective and eco-friendly biosorption technology for complete removal of nickel ions from an aqueous solution: Optimization of process variables

https://doi.org/10.1515/gps-2022-0064
received March 10, 2022; accepted May 02, 2022

Abstract: The enormous industrial usage of nickel during its manufacture and recycling has led to widespread environmental pollution. This study was designed to examine the ability of *Gelidium amansii* biomass to biosorb Ni^{2+} ions from an aqueous solution. Six independent variables, including contact time (1.0 and 3.0 h), pH (4 and 7), Ni^{2+} concentration (25 and 200 mg·L^{-1}), temperature (25°C and 50°C), *G. amansii* biomass (1.0 and 4.0 g·L^{-1}), and agitation mode (agitation or static), were investigated to detect the significance of each factor using a Plackett–Burman design. The analysis of variance for the Ni^{2+} biosorption percentage indicated that three independent variables (contact time, temperature, and agitation–static mode) exhibited a high level of significance in the Ni^{2+} biosorption process. Twenty experiments were conducted containing six axial, eight factorial, and six replicates points at center points. The resulting face-centered central composite design analysis data for the biosorption of Ni^{2+} exhibited a very large variation in the removal percentage of Ni^{2+}, which ranged from 29.73 to 100.00%. The maximum Ni^{2+} biosorption percentage was achieved in the 16th run with an experimental percentage quantified as 100.00% under the experimental conditions of 3 h of incubation time and 45°C with 100 rpm for agitation speed.

Keywords: *Gelidium amansii*, bioremediation, optimization, Plackett–Burman design, FCCCD analysis

1 Introduction

Water contamination is one of the global concerns as it is the main requirement for living organisms and human livelihood, and also the rapid rise of freshwater insufficiency and its limited availability increase additional environmental stresses [1]. The environment has been polluted with different pollutants such as organic, inorganic pollutants, radioactive isotopes, and gaseous pollutants [1]. Heavy metal pollution is one of the most environmental contaminants that need special attention and effective strategies among the different kinds of water pollution due to its toxicity, long residence, nonbiodegradable nature, and uncontrolled dispersion [2,3]. Heavy metal elements exist naturally on the Earth's crust during the Earth's formation, but anthropogenic activities such as metal mining, using of chemical fertilizers, and industrial manufacturing resulted in an imminent surge of metallic substances in both the terrestrial and the marine environments [4,5]. Nickel (Ni) is a naturally arising element in great capacity in the earth's crust and core and can cause natural pollution to surface water and soil, but this is mainly due to industrial and mining

* **Corresponding author: Ragaa A. Hamouda,** Department of Biology, College of Sciences and Arts Khulais, University of Jeddah, Jeddah 21959, Saudi Arabia; Microbial Biotechnology Department, Genetic Engineering and Biotechnology Research Institute, University of Sadat City, Sadat City, 22857, Menoufia Governorate, Egypt, e-mail: ragaa.hamouda@gebri.usc.edu.eg, ragaahom@yahoo.com
Noura El-Ahmady El-Naggar, Nashwa H. Rabei: Department of Bioprocess Development, Genetic Engineering and Biotechnology Research Institute, City of Scientific Research and Technological Applications (SRTA-City), Alexandria, 21934, Egypt
Muhammad A. Abuelmagd: Department of Botany, Faculty of Science, Mansoura University, Mansoura, Egypt
Maha M. Alharbi: Department of Biology, Faculty of Science, University of Tabuk, Tabuk, Saudi Arabia
Doaa Bahaa Eldin Darwish: Department of Botany, Faculty of Science, Mansoura University, Mansoura, Egypt; Department of Biology, Faculty of Science, University of Tabuk, Tabuk, Saudi Arabia
Safinaz A. Farfour: Department of Environmental Biotechnology, Genetic Engineering and Biotechnology Research Institute, University of Sadat City, Sadat City, Egypt

Open Access. © 2022 Noura El-Ahmady El-Naggar *et al.*, published by De Gruyter. This work is licensed under the Creative Commons Attribution 4.0 International License.

activities [6]. Although nickel is an important biological element for the normal growth of several species of organisms, its increased amounts can cause toxic effects such as respiratory disorders, kidney inflammation, and extreme general weakness, and has been concerned as a probable carcinogen [7]. Nickel is one of the more toxic elements due to high solubility in the marine ecosystem, and it is simply absorbed by living organisms [8,9]. Individuals consume nickel and its derivative compounds through drinking water, food, air, tobacco, nickel-plated materials, and some medical body parts [7]. Nickel is found in the wastewater of different activities like electroplating, paint formulation, mineral processing, thermal power plants, porcelain enameling, and storage battery manufacture [10,11]. The acceptable concentration limit of nickel in the industrial effluent in wastewater is 2.0 $mg{\cdot}L^{-1}$, and meanwhile, the concentration limit in the drinking water is only 0.01 $mg{\cdot}L^{-1}$ [8]. Removal of highly elevated concentrations of nickel to its acceptable limited range with cost-effective and environmental friendly techniques becomes an urgent need. Biological techniques, based on living microorganisms, nonliving dry matter, or even plants, can minimize the toxic heavy metal levels to their naturally acceptable limits in a cost-effective and environmentally friendly manner [12]. Biosorption is an energy-independent process in which heavy metal elements are adsorbed on the cell surface from wastewater using biomass of microorganism, seaweed, and plant residues or their polymeric substances; hence, it provides a renewable, reusable, and very cost-effective technique [13,14]. Marine life has huge biodiversity, and macroalgae (seaweeds) are one such group and are identified as a promising biosorbent due to their ability to produce phycocolloids compounds such as alginates and agar [15]. Seaweeds have considerable advantages such as natural origin, low cost, ready abundance of biomass, and effectiveness against a wide range of pollutants [16]. Alginic acid and fucoidan (sulfated polysaccharides) are essential compounds as they contain the functional groups that play a vital role in the biosorption of heavy metals. The cell wall of red algae contains cellulose that had biosorption capacities but is attributed to the presence of sulfated polysaccharides made of galactans [14,15]. The marine algal surface has high metal binding capacities due to the presence of the high amount of biological compounds such as polysaccharides, proteins, and lipids in the cell wall structure that contains the abundant number of the binding moiety functional groups, for example, carboxyl, hydroxyl sulfuryl, and sulfate, which act as connecting sites for heavy metals [16]. The brown, red, and numerous green algal cell walls are included in a fibrillar skeleton and an amorphous surrounding matrix and also contain sulfated polysaccharides (fucoidan) or alginate that are responsible for binding heavy metals related to the stereochemical effects [17]. Red algae cell walls consist of galactanes (sulfated polysaccharides), which are also responsible for the complexion with metal ions [18]. Hence, seaweeds have several benefits such as high-efficiency metal elimination, nontoxic, and low cost [16]. The red alga *Gelidium amansii* was removed 100% of Pb^{2+} from the aqueous solution with 200 $mg{\cdot}L^{-1}$ Pb^{2+} [19].

This research aimed to statistically optimize the dry biomass of macro-red alga, *G. amansii*, and investigate its potentiality as a cost-effective biosorbent for the removal of nickel ions. The biomass of *G. amansii* is characterized before and after the biosorption process of nickel by scanning electron microscope (SEM) and Fourier-transform infrared spectroscopy (FTIR) analyses.

2 Materials and methods

2.1 Gathering and preparation of the biosorbent (marine alga)

G. amansii (red alga) used in this study was obtained from the Mediterranean Sea coast of Abu-Qir, Alexandria, Egypt, in July 2020. External sand and salts were removed by washing the collected biomass of *G. amansii* with running tap water followed by double immersion in distilled water. *G. amansii* biomass was ground with a blender to produce particles with sizes ranging from 1–1.2 mm and sieved using a standard laboratory test sieve (Endecotts/Ltd., London, England) after drying in an oven at 65°C for 3 days. Then, 20 grams of ground *G. amansii* biomass was mixed with distilled (1 L) and the suspension was stirred at ambient temperature for approximately 30 min. Finally, algal biomass was filtered with Whatman filter paper no. 1 and dried at 65°C for 3 days, and steady weight was achieved and then kept at 4°C for further use in the biosorption process.

2.2 Preparation of nickel solution

Ni^{2+} aqueous solutions were concocted by dissolving $Ni(NO_3)_2{\cdot}6H_2O$ in deionized water, and the purity of $Ni(NO_3)_2{\cdot}6H_2O$ was 99.995%. The pH was adjusted by the appropriate addition of 0.1 M HCl or NaOH solutions.

2.3 Design of screening experiments for Ni^{2+} biosorption using Plackett–Burman design

Plackett–Burman design (PBD) is an effective inspection tool to determine the noteworthy variables between different reacted variables that affect a process. PBD was recycled for the selection of the variables that had a noteworthy influence, either positively or negatively, on Ni^{2+} biosorption out of six reacted independent variables. The six independent virtual factors included different incubation times (1 and 3 h), two different initial pH levels (4 and 7), Ni^{2+} concentrations (25 and 200 mg·L^{-1}), temperatures (25°C and 50°C), *Gelidium amansii* biomass concentrations (1 and 4 g·L^{-1}), and static or agitation conditions. Each variable was examined at two levels: low (−1) and high (1) levels. Twelve PBD runs were performed to assess the influence of the six selected factors on the Ni^{2+} biosorption efficiency. In the tentative design, each row signifies an experiment, and each column exemplifies an independent factor (Table 1). PBD is performed using the first-order model equation:

$$Y = \beta 0 + \sum \beta i Xi \quad (1)$$

where Y is the response value of the Ni^{2+} biosorption percentage, β_0 is the model intercept, β_i is the linear coefficient, and X_i is the level of the independent factors. *G. amansii* biomass was blended with a solution of Ni^{2+}, and the experiments were performed either wise static or with agitation for a definite incubation time at the designated temperature.

2.4 Design of statistical optimization for nickel (Ni^{2+}) biosorption using FCCCD

Based on the resulting data from the PBD experimental design, three significant factors (contact time, temperature, and agitation speed) with three codes (−1, 0, and 1) were specified for each variable and marked. A five-level face-centered central composite design (FCCCD) was designed to detect and describe the optimum circumstances of the important factors, the individual factors, and the relationship between the particular factors with elevated effects on Ni^{2+} biosorption. The three factors selected from PBD for further optimization using FCCCD were contact time, temperature (°C), and agitation speed, which were denoted as X_1, X_2, and X_3, respectively. FCCCD had 20 different tests generated with Design-Expert version 7 for Windows software.

The interaction between Ni^{2+} biosorption (Y) and the significant independent variables (X_1, X_2, and X_3) is given by the following second-order polynomial equation:

$$Y = \beta_0 + \sum_i \beta_i X_i + \sum_{ii} \beta_{ii} X_i^2 + \sum_{ij} \beta_{ij} X_i X_j \quad (2)$$

where Y is the predicted Ni^{2+} biosorption, β_0 is the regression coefficient, β_i is the linear coefficient, β_{ii} is the

Table 1: Twelve-trial Plackett–Burman experimental design for evaluation of independent variables with coded and actual levels along with the observed and predicted values of Ni^{2+} biosorption by *Gelidium amansii* biomass

Std	Run	Coded and actual levels of the independent variables						Ni^{2+} removal (%)		Residuals
		Contact time	Ni^{2+} conc.	pH	Temperature	Biomass	Agitation–static	Actual	Predicted	
12	1	−1	−1	−1	−1	−1	−1	97.65	97.67	−0.02
7	2	−1	1	1	1	−1	1	99	99.03	−0.03
5	3	1	1	−1	1	1	−1	98.36	98.39	−0.03
10	4	1	−1	−1	−1	1	1	98.6	98.62	−0.02
2	5	1	1	−1	1	−1	−1	98.6	98.57	0.03
1	6	1	−1	1	−1	−1	−1	98.22	98.21	0.01
3	7	−1	1	1	−1	1	−1	97.82	97.76	0.06
8	8	−1	−1	1	1	1	−1	97.91	97.96	−0.05
9	9	−1	−1	−1	1	1	1	98.62	98.56	0.06
6	10	1	1	1	−1	1	1	98.88	98.90	−0.02
11	11	−1	1	−1	−1	-1	1	98.54	98.55	−0.01
4	12	1	−1	1	1	−1	1	99.31	99.29	0.02

Level	Hours	mg·L^{-1}	pH	°C	g·L^{-1}	Agitation–static
−1	1	25	4	25	1	Agitation
1	3	200	7	50	4	Static

quadratic coefficient, and β_{ij} is the interaction coefficient, and X_i is the coded level of the independent variable.

2.5 Statistical analysis

The statistical analysis and experimental designs were achieved using Minitab and Design Expert version 7 for Windows software. The regression model of the resulting actual data was achieved to estimate the analysis of variance. The contribution % of each variable was also calculated. To design the 3D surface plots, the statistical software package STATISTICA software (version 8.0, StatSoft Inc., Tulsa, OK) was used. Meanwhile, contour plots and response surfaces were used to measure the interaction between the various significant variables. The analysis of variance (ANOVA) significance of the variable mean differences was prescribed ($p \leq 0.05$).

2.6 Analytical methods

The analysis of Ni^{2+} in the filtered solutions (0.2 µm polyterafluorethylene syringe filters) was done using inductively coupled plasma-atomic emission spectroscopy (ICP-AES, Thermo Scientific). The biosorption experimental data were obtained in triplicate ($n = 3$). Meanwhile, the ability of *G. amansii* biomass to biosorb Ni^{2+} ions was estimated using the following equation:

$$\text{Biosorption efficiency (\%)} = \frac{(C_i - C_f)}{C_i} \times 100 \quad (3)$$

where C_i is the initial Ni^{2+} ion concentration ($mg{\cdot}L^{-1}$) and C_f is the residual Ni^{2+} ion concentration ($mg{\cdot}L^{-1}$).

2.7 Biosorbent characterization (*G. amansii* biomass)

Alga *G. amansii* biomasses were analyzed before and after biosorption process Ni^{2+} using FTIR spectral analysis, energy-dispersive spectroscopy (EDS) analysis, and SEM.

2.8 FTIR spectral analysis

FTIR analyses were performed to interpret the distinct chemical functional groups of the *G. amansii* biomass samples that may be accountable for the biosorption of Ni^{2+} *G. amansii* biomass analyzed before and after the Ni^{2+} biosorption process using FTIR spectroscopy (Thermo Fisher Nicolete IS10, USA spectrophotometer). The FTIR spectrum was analyzed over a spectral range from 400 to 4,500 cm^{-1}.

2.9 Scanning electron microscopy

Gelidium amansii biomass samples before and after Ni^{2+} biosorption were scanned to illustrate the morphological changes and to demonstrate Ni^{2+} biosorption. *G. amansii* biomass samples were crusted with gold and inspected at various magnifications at 20 kV at Electron-Microscope-Unit of Mansoura University, Egypt.

2.10 EDX analysis

Energy-dispersive X-ray spectroscopy (EDX) analysis is an effective analytical tool that is used for the elemental analysis of *G. amansii* biomass before and after the biosorption process using an Oxford X-Max 20 Instrument at Electron Microscope Unit, Faculty of Science, Alexandria University, Alexandria, Egypt.

3 Results and discussion

3.1 PBD experimental results and detection of significant variables

In the current survey, Ni^{2+} was removed using *G. amansii* as a biosorbent and PBD as an analytical screening method to detect the significance of multiple independent factors that influenced the biosorption process. The actual and coded levels of six independent variables, including contact time (1.0 and 3.0 h), pH (4 and 7), Ni^{2+} concentration (25 and 200 $mg{\cdot}L^{-1}$), temperature (25°C and 50°C), *G. amansii* biomass (1.0 and 4.0 $g{\cdot}L^{-1}$), and agitation mode (agitation or static), were coded using (–1 and 1) for each variable factor, as presented in Table 1.

The data (Table 1) illustrate that the maximum biosorption percentage for Ni^{2+} was achieved in the 12th run, with percentages quantified as 99.31% and 99.29% for the actual and predicted values, respectively, followed by the

2nd run, which recorded biosorption percentages quantified as 99% and 99.03% for the actual and predicted values, respectively. Meanwhile, the 1st run recorded the minimum biosorption percentage. The maximum biosorption percentage was achieved at 3 h of contact time, 25 mg·L^{-1} (Ni^{2+} initial concentration), pH value (7), 50°C, and 1.0 g·L^{-1} (*G. amansii* biomass) under static conditions. PBD was also conducted to define the most significant factors affecting the Ni^{2+} biosorption percentage from aqueous solutions using *G. amansii* biomass, as illustrated in Table 1.

The correlation between the Ni^{2+} biosorption percentage and the other independent factors was investigated with respect to their effects on the Ni^{2+} biosorption process via PBD, as illustrated in Table 2. The coefficient values for each reaction factor exhibit the extent of the effect of this factor on the Ni^{2+} biosorption process. The analysis of the regression coefficients and the cumulative effects of the six interacting factors (Table 2 and Figure 1) show that five factors, including contact time (A), Ni^{2+} concentration (B), pH value (C), temperature (D), and agitation mode (F), had coefficient values quantified as 0.20, 0.07, 0.06, 0.17, and 0.37 with contribution percentages calculated as 20.833, 7.292, 6.250, 17.708, and 38.542, respectively, and had the positive effects on the Ni^{2+} biosorption process, which means that the increase in these factors could enhance a positive effect on Ni^{2+} biosorption. Conversely, *G. amansii* biomass exhibited the negative effects, which means that the decrease in *G. amansii* biomass concentration could enhance a positive effect on the Ni^{2+} biosorption process. The effect of each variable on the Ni^{2+} biosorption process is illustrated in Table 2 and Figure 1. High values, either positive or negative, indicate that the factor plays a key role and has an effective function on the Ni^{2+} biosorption process, while low values (approximately zero) reflect a noneffective on the biosorption process.

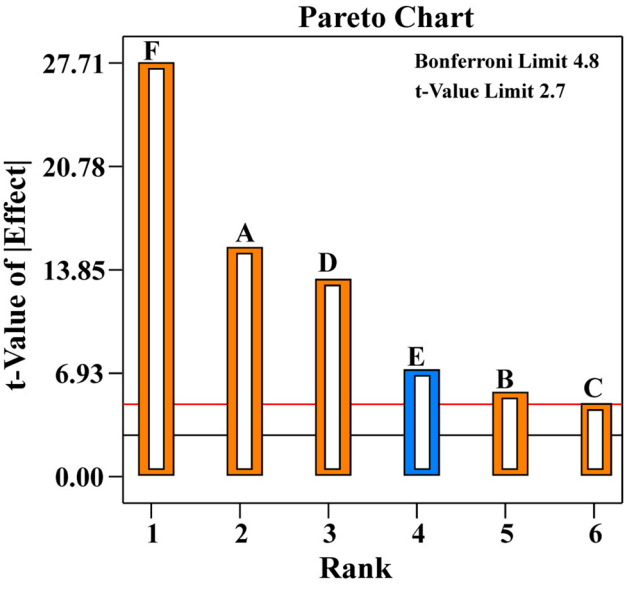

Figure 1: Pareto chart indicating the cumulative effects of independent variables on Ni^{2+} removal by *G. amansii* biomass using Plackett–Burman design: the orange and blue colors represent the positive and negative independent variables, respectively.

Results indicated that the optimum pH value for maximum absorption of Ni^{2+} by red alga *G. amansii* was at near 7, and the same results were obtained when *Aspergillus niger*, *Cystoseria indica*, and *Rhizopus arrhizus* were applied, and the maximum biosorption was at pH 6, but in the case of *Acinetobacter baumannii* UCR-2971, the pH level was 4.5 [20–23]. It took nearly 3 h for optimum

Table 2: Regression statistics and ANOVA for the experimental results of the Plackett–Burman design used for Ni^{2+} biosorption by *G. amansii* biomass

Term	Coefficient	Effect	% Contribution	*F*-value	*P*-value prob > *F*
Intercept	98.46			164.76	<0.0001
Contact time (A)	0.20	0.40	20.833	181.24	<0.0001
Ni^{2+} concentration (B)	0.07	0.14	7.292	24.31	0.0044
pH (C)	0.06	0.12	6.250	18.20	0.0080
Temperature (D)	0.17	0.34	17.708	134.07	<0.0001
Biomass (E)	−0.09	−0.18	9.375	39.19	0.0015
Agitation–static (F)	0.37	0.74	38.542	591.53	<0.0001
Std. Dev.	0.05	R^2		0.9950	
Mean	98.46	Adj R^2		0.9889	
C.V. (%)	0.05	Pred R^2		0.9710	
PRESS	0.08	Adeq Precision		40.54	

Significant values, df: degree of freedom, *F*: Fishers's function, *P*: level of significance.

Ni^{2+} biosorption, and these results are nearly approved by Rodrígue and Quesada [23], and they also reported that the absorption of Ni^{2+} by *Acinetobacter baumannii* UCR-2971 was achieved after 100 min, pH 4.5, with biomass of 4.0 $g{\cdot}L^{-1}$ (Table 3).

3.2 The adequacy of the model

The model should be validated before its acceptance as a statistically accurate model, and a normal probability plot (NPP) illustrates the normal distribution of the residuals to test the model's accuracy and adequacy [24]. Figure 2 shows the analyzed data to test the normality of residuals, whereas the NPP of the residuals and residuals vs predicted for Ni^{2+} biosorption by *G. amansii* biomass was determined using the first-order polynomial equation. The residuals are defined as the differences between the experimental values of the responses and those predicted by the theoretical model. The closer residuals to the straight line with low residual values indicate that the data did not exhibit any abnormal action and achieved a very accurate prediction model [18,25].

Figure 2 displays the NPP of the residuals against the predicted values of the model. The data exhibit a normal distribution and demonstrate the model validity, as the residual points on the diagonal line are found close to each other.

3.3 Regression statistics and ANOVA for PBD

The model determination coefficient (R^2) was 0.9950, which means that 99.59% of the variation in Ni^{2+} biosorption was dependent on the independent factors and that only 0.05% of the variation could not be explained by the regression model. A regression model with a high R^2 value greater than 0.9 is considered to be highly

Table 3: Face-centered central composite design representing the response of Ni^{2+} removal % by *G. amansii* as influenced by contact time (X_1), temperature (X_2), and agitation speed (X_3) along with the predicted Ni^{2+} removal % and residuals and the actual factor levels corresponding to coded factor levels

Std	Run	Type	Variables			Ni^{2+} removal (%)		Residuals
			X_1	X_2	X_3	Experimental	Predicted	
19	1	Center	0	0	0	95.37	94.82	0.55
2	2	Fact	1	−1	−1	89.88	89.69	0.19
20	3	Center	0	0	0	97.19	94.82	2.37
1	4	Fact	−1	−1	−1	78.23	77.70	0.54
17	5	Center	0	0	0	94.11	94.82	−0.71
16	6	Center	0	0	0	94.98	94.82	0.16
12	7	Axial	0	1	0	79.73	81.14	−1.41
11	8	Axial	0	−1	0	75.30	76.70	−1.40
6	9	Fact	1	−1	1	29.73	29.70	0.03
18	10	Center	0	0	0	96.40	94.82	1.58
10	11	Axial	1	0	0	86.07	86.51	−0.44
5	12	Fact	−1	−1	1	66.99	66.33	0.65
9	13	Axial	−1	0	0	95.31	97.69	−2.38
15	14	Center	0	0	0	96.51	94.82	1.69
7	15	Fact	−1	1	1	76.33	75.81	0.52
13	16	Axial	0	0	−1	100.00	101.45	−1.45
3	17	Fact	−1	1	−1	75.51	74.83	0.68
8	18	Fact	1	1	1	41.61	41.44	0.17
14	19	Axial	0	0	1	70.57	71.94	−1.37
4	20	Fact	1	1	−1	89.15	89.09	0.05

Variable	Variable code	Coded and actual levels		
		−1	0	1
Contact time (h)	X_1	2	3	4
Temperature (°C)	X_2	30	45	60
Agitation speed (rpm)	X_3	100	150	200

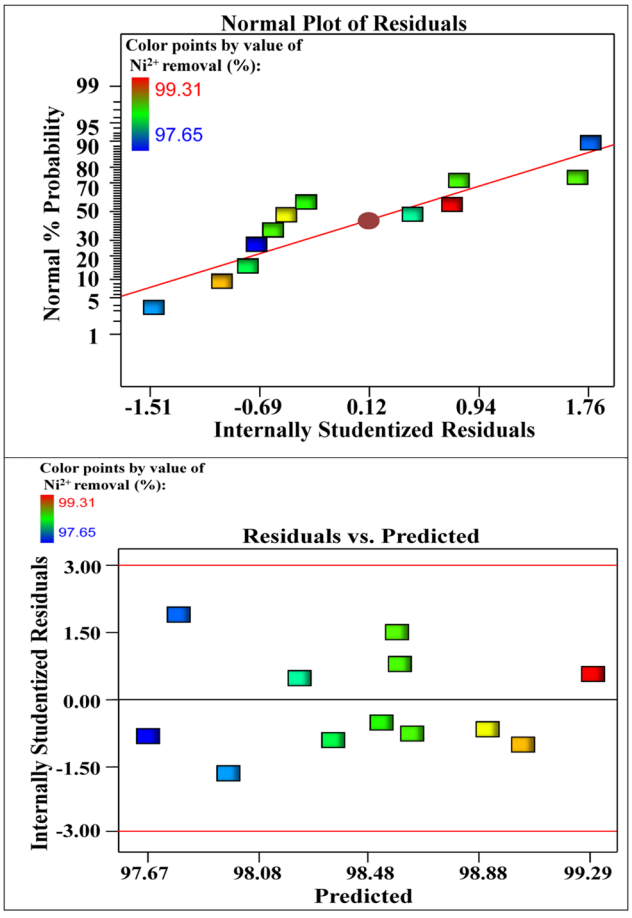

Figure 2: NPP of the residuals and residuals vs predicted Ni^{2++} removal by *Gelidium amansii* biomass determined by the first-order polynomial equation.

correlated, and the model is adequate to interpret the difference in the experimental data and theoretical values [26]. For further interpretation and assessment of the significance of the interacting variables on the Ni^{2+} biosorption process, the obtained data were analyzed statistically in terms of ANOVA. The relationship between the six independent factors and Ni^{2+} biosorption was determined using a multiple-regression model (Table 2). The adequacy of the model was tested by the estimation of the coefficient (R^2 value), which is generally between 0.0 and 1.0. The model is considered to be strong and effective if the R^2 value is closer to 1.0. Table 2 illustrates the adjusted determination coefficient (Adj. R^2) and predicted (Pred. R^2) values quantified as 0.9889 and 0.9710, respectively, which are considered to be very large values and illustrate a highly significant model and its suitability to interpret the interaction between reacted variables and the Ni^{2+} biosorption percentage using *G. amansii* biomass. The calculated Adeq. The precision fraction (40.54) specifies a sufficient signal-to-noise ratio.

The experimental PBD data were fitted with a first-order polynomial equation that signified the Ni^{2+} biosorption percentage as a function of the incubation time, Ni^{2+} concentration, pH value, temperature, *G. amansii* biomass, and agitation–static mode.

Based on the ANOVA for the Ni^{2+} biosorption percentage (Table 2), correlation significance indicated that some independent variables (contact time, temperature, agitation–static mode) exhibited a high level of significance ($P < 0.0001$), while other factors (Ni^{2+} concentration, pH level, and *G. amansii* biomass) displayed relatively low levels of significance ($P = 0.0044$, 0.0080, and 0.0015).

3.4 Optimization of Ni^{2+} biosorption via FCCCD

The influence of the three significant independent variables (contact time, temperature, and agitation speed) was investigated. Applying FCCCD statistics illustrated the interaction between three variables and their optimal conditions for achieving the maximum bioadsorption percentage. By applying FCCCD and holding three parameters at three different levels, a total of 20 bioadsorption tests were performed, as illustrated in Table 3, which demonstrates the actual, predicted, and residual values for Ni^{2+} biosorption. A face-centered central composite matrix was also conducted to examine the interactive, individual, and quadratic effects of selected variables in the biosorption of Ni^{2+} using dry *G. amansii* biomass. Different combinations are represented in Table 3 (X_1: incubation time, X_2: temperature, and X_3: agitation speed). Twenty experiments were conducted containing six axial points, eight factorial points, and six replicates at center points. The resulting FCCCD analysis data for the biosorption of Ni^{2+} exhibited a very large variation in the removal percentage of Ni^{2+}, which ranged from 29.73% to 100.00%. The maximum Ni^{2+} biosorption percentage was achieved in the 16th run with an experimental percentage quantified as 100.00% under the experimental conditions of 3 h of incubation time and 45°C and 100 rpm for agitation speed. The actual and predicted values of yields of Ni^{2+} biosorption are also illustrated in Table 3.

3.5 Multiple regression analysis and ANOVA for FCCCD

The Ni^{2+} biosorption percentage was statically analyzed using multiple regression analysis of the FCCCD model

Table 4: Analysis of variance for biosorption of Ni^{2+} ions by *Gelidium amansii* biomass from aqueous solution obtained by FCCCD

Source of variance	Degrees of freedom	Sum of square	Mean of square	*F*-value	*P*-value	Coefficient estimate	
Model		1	6,598.70	733.19	270.46	<0.0001	94.82
Linear effect	X_1	1	312.91	312.91	115.43	<0.0001	−5.59
	X_2	1	49.29	49.29	18.18	0.0017	2.22
	X_3	1	2,176.80	2,176.80	802.99	<0.0001	−14.75
Interaction effect	X_1X_2	1	2.57	2.57	0.95	0.3536	0.57
	X_1X_3	1	1,182.67	1,182.67	436.27	<0.0001	−12.16
	X_2X_3	1	76.20	76.20	28.11	0.0003	3.09
Square effect	X_1^2	1	20.37	20.37	7.52	0.0208	−2.72
	X_2^2	1	694.95	694.95	256.36	<0.0001	−15.90
	X_3^2	1	181.62	181.62	67.00	<0.0001	−8.13
Error effect	Lack of Fit	5	20.61	4.12	3.17	0.1155	
	Pure Error	5	6.50	1.30			
R^2	0.9959	Std. dev.	1.65				
Adj. R^2	0.9922	Mean	81.45				
Pred. R^2	0.9844	C.V. [%]	2.02				
Adeq. precision	61.63	PRESS	103.64				

Significant values, *F*: Fisher's function, *P*: level of significance, C.V.: coefficient of variation.

and ANOVA, as illustrated in Tables 4 and 5. The analysis demonstrates the coefficient values, determination coefficient (R^2) to detect the effectiveness of the polynomial regression model, the adjusted and predicted R^2 values, the effect of each factor, probability *P* value, and Fisher test (*F*-test). Linear (X_1, X_2, and X_3), interactions (X_1X_2, X_1X_3, and X_2X_3), and quadratic effects (X_1^2, X_2^2, and X_3^2) of the three interacting process factors were also assessed.

The coefficient of determination (R^2) of the model was calculated to be 0.9959 (Table 4), proving that 99.59% of the variation in the biosorption percentage of Ni^{2+} was attributed to the interacting variables and that

Table 5: Fit summary for FCCCD for biosorption of Ni^{2+} ions by *Gelidium amansii* biomass from aqueous solution

Lack of fit tests					
Source	**Sum of squares**	***df***	**Mean²**	***F*-value**	***P*-value prob > *F***
Linear	4,080.32	11	370.94	285.34	<0.0001
2FI	2,818.89	8	352.36	271.05	<0.0001
Quadratic	20.61	5	4.12	3.17	0.1155
Sequential model sum of squares					
Source	**Sum of squares**	***df***	**Mean²**	***F*-value**	***P*-value prob > *F***
Linear vs mean	2,538.99	3	846.33	3.31	0.0469
2FI vs linear	1,261.44	3	420.48	1.93	0.1739
Quadratic vs 2FI	2,798.28	3	932.76	344.08	<0.0001
Model summary statistics					
Source	**Standard deviation**	**R^2**	**Adjusted R^2**	**Predicted R^2**	**PRESS**
Linear	15.98	0.3832	0.2675	−0.1906	7,888.57
2FI	14.74	0.5736	0.3768	−1.9630	19,632.46
Quadratic	1.65	0.9959	0.9922	0.9844	103.64

Significant values, df: degree of freedom, PRESS: sum of squares of prediction error, two factor interaction: 2FI.

only 0.41% of the variation could not be interpreted via the model. A regression model with an R^2 value is greater than 0.9, which was considered to be strongly correlated [10]. The highest R^2 value also illustrates a good relation between the experimental data and the predicted values generated by model Box and Draper [27].

The optimum correlation between the expected and experimental values of Ni^{2+} biosorption was designated by a reasonable correlation between the Pred. R^2 of 0.9844 and the Adj. R^2 of 0.9922. Adeq. precision with a ratio of 61.63 shows an adequate sign-to-noise ratio. Predicted residual sum of squares (PRESS) and CV values were quantified as 103.64 and 2.02, respectively, while the low value of CV indicated good precision of the experimental performance [27]. This model also displays standard deviations and mean values calculated as 1.65 and 81.45, respectively (Table 4). The presence of negative coefficient values (Table 4) suggests a reverse correlation among the factors, while the positive values suggest a synergistic relationship between the factors [28]. Subsequently, the negative coefficient values of the linear, interaction, and square effects of the three process parameters mean that they have a negative effect on the Ni^{2+} biosorption process by *G. amansii* biomass, while the positive coefficient values mean that they enhance the Ni^{2+} percentage by *G. amansii* biomass in the tested ranges of the selected three process factors. Table 4 indicates that the linear effect of X_2 and the interaction effect of X_1X_2 and X_2X_3 had a positive effect on the Ni^{2+} biosorption process, while the linear effect of X_1 and X_3, the interaction effect of X_1X_3, and the square effect of X_1^2, X_2^2, and X_3^2 had a negative effect on the biosorption process. To estimate the correlation between dependent and independent factors and to detect the optimum conditions for Ni^{2+} biosorption percentage, the three interacting variables X_1 (contact time), X_2 (temperature), and X_3 (agitation speed), and a second-order polynomial regression model was suggested to estimate the maximum levels of three variables and detect the predicted response (Y) in terms of the independent process factors as follows:

$$\begin{aligned}\text{The predicted value of the } Ni^{2+} \text{ biosorption percentage } (Y) \\ = 94.82 - 5.59X_1 + 2.22X_2 - 14.75X_3 \\ + 0.57X_1X_2 - 12.16X_1X_3 \\ + 3.09X_2X_3 - 2.72X_1^2 - 15.90X_2^2 - 8.13X_3^2\end{aligned} \quad (4)$$

where Y is the predicted value of the Ni^{2+} biosorption percentage, X_1 is the contact time, X_2 is the temperature, and X_3 is the agitation speed.

The ANOVA of the FCCCD, as well as the mean square, the sum of square, F-value, P-value, and confidence level, was calculated. The corresponding probability values (P values) are shown in Table 4 and used to explain and clarify the significance of each coefficient, which is a key point to recognize the pattern of the interaction between the tested factors. Lower P values exhibit more significance in the corresponding coefficient. The current ANOVA data (Table 4) show that Fisher's F test is 270.46, and a very low probability value was quantified ($P < 0.0001$). Both values prove that the model is highly significant for the Ni^{2+} biosorption process. Furthermore, variables with confidence levels greater than 90% and P values less than 0.1 were considered to be significant [29]. Therefore, the linear, interaction, and square coefficient terms had very significant effects ($P < 0.1$) on the Ni^{2+} biosorption process, except that the interaction effect between incubation time and temperature (X_1X_2) had no significant contribution to the Ni^{2+} biosorption process. The current model recorded an adequate precision value quantified as 61.63, while the PRESS value was calculated as 103.64.

Table 5 presents the fit summary data applied to detect the maximum polynomial model among the linear, interaction, and square models appropriate for the experimental results. The fitting model was selected depending on both the significant model terms and nonsignificant lack of fit test [28]; moreover, the statistics of the model summary focused on the model with lower SD and higher adjusted and predicted R^2. The current fit summary data (Table 5) revealed that the quadratic model is a very significant and adequate model fitting the FCCCD of the Ni^{2+} biosorption percentage using *G. amansii* biomass from the aqueous solution and has a very low P value of less than 0.0001. Moreover, the lack of fit F value and probability P value are not significant (quantified as 3.17 and 0.1155, respectively). The summary statistics of the model displayed the minimum value of standard deviation (1.65), the largest adjusted R^2 value of 0.9922, and a predicted R^2 of 0.9844.

3.6 Three-dimensional plots for Ni^{2+} biosorption

The 3D graphs were plotted to demonstrate the pairwise combination of the selected independent variables and the Ni^{2+} biosorption percentage on the z-axis against two independent factors, while the other factors were held at the zero level. Graphs 3D illustrate the change in the response surface and detect the ideal levels of three selected process factors for achieving the maximum

biosorption percentage from Ni^{2+} using *G. amansii* biomass. Figure 3a–c demonstrate the three-dimensional plots generated for Ni^{2+} biosorption percentages as a function of contact time, temperature, and agitation speed.

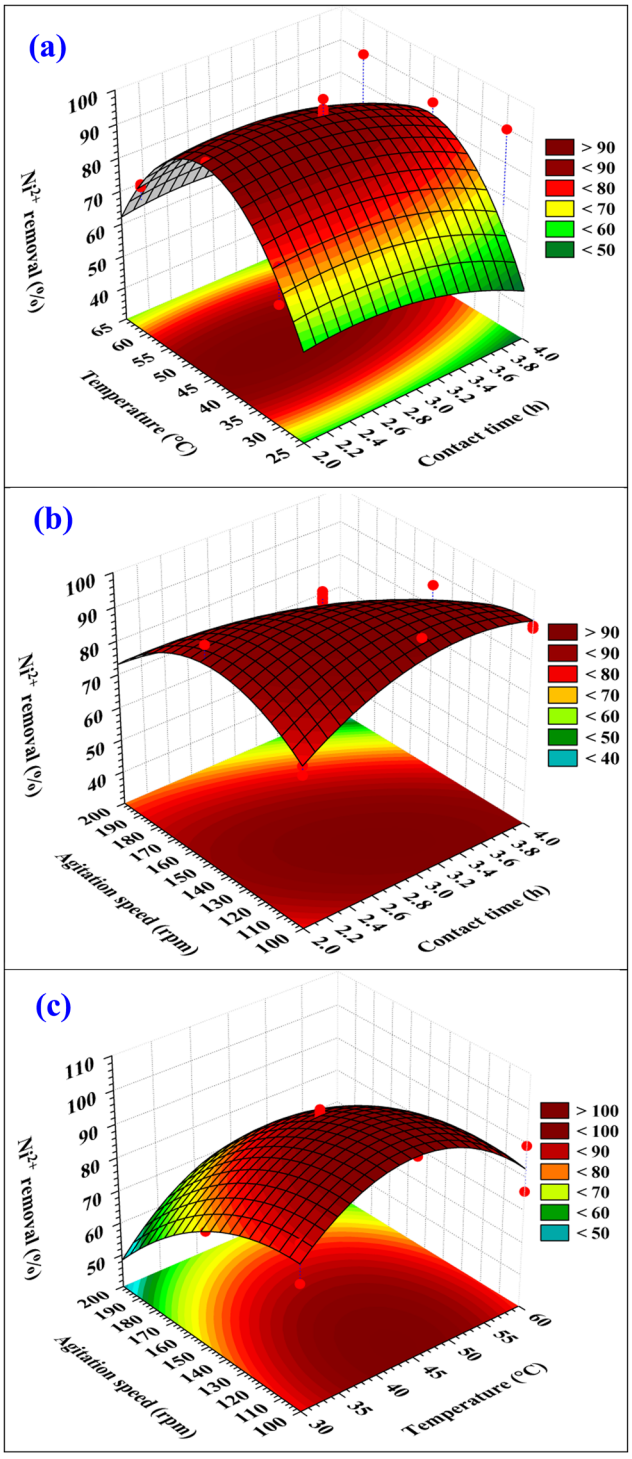

Figure 3: Three-dimensional surface plot for biosorption of Ni^{2+} ions by *G. amansii* biomass from aqueous solution, showing the interactive effects of the three tested variables: (a) agitation speed, (b) temperature, and (c) contact time was held at their zero.

Figure 3a represents the effect X_1 (contact time) and X_2 (temperature), while X_3 (agitation speed) was held at their zero (center) levels (150 rpm). The maximum Ni^{2+} biosorption percentage appeared at moderate temperature and contact time, whereas the Ni^{2+} biosorption percentage increased with increasing temperature and increasing incubation time until the midpoint; however, a greater increase in the temperature and incubation time caused a gradual decrease in the Ni^{2+} biosorption percentage.

Figure 3b represents the effects X_3 (agitation speed) and X_1 (contact time), while X_2 (temperature) was held at their zero (center) levels (45°C). The maximum Ni^{2+} biosorption percentage appeared at moderate contact time and agitation speed, whereas the Ni^{2+} biosorption percentage increased with increasing contact time and increasing agitation speed until the midpoint; however, a greater increase in the contact time and agitation speed resulted in a gradual decrease in the Ni^{2+} biosorption percentage.

Conversely, Figure 3c represents the holding of contact time at zero level (3 h) and studies the effect of two other factors (agitation speed and temperature) on the Ni^{2+} biosorption percentage. It also revealed that the maximum Ni^{2+} biosorption percentage appeared at moderate temperature and agitation speed, whereas the Ni^{2+} biosorption percentage increased with increasing temperature and increasing agitation speed until the midpoint; however, a greater increase in the temperature and agitation speed resulted in a gradual decrease in the Ni^{2+} biosorption percentage.

The biosorption percentage of Ni^{2+} was elevated by increasing the incubation time from 2 to 3 h, which could be a result of the availability of Ni^{2+} ion reaching sites in the biosorbent with time [30]. However, the decrease in the Ni^{2+} biosorption percentage observed at 4 h was caused by the repulsion powers between solute molecules and the bulk phase, and the remaining surface sites became saturated [31,32]. The decrease in the Ni^{2+} biosorption percentage could also be explained in the view of Liu et al. [33] who attributed this decrease to the interaction between the functional groups allocated on the biosorbent surface and intercellular accumulation.

Temperature plays a key role in the biosorption process as it affects the viscosity and kinetic energy of metal ions in the solution and hence the diffusion rate as well as the metal ion binding capacity to the biosorbent [34]. The effect of temperature on the heavy metal biosorption process can be negligible, positive, or negative [35], although elevated temperatures can cause physical damage to the biosorbent [34].

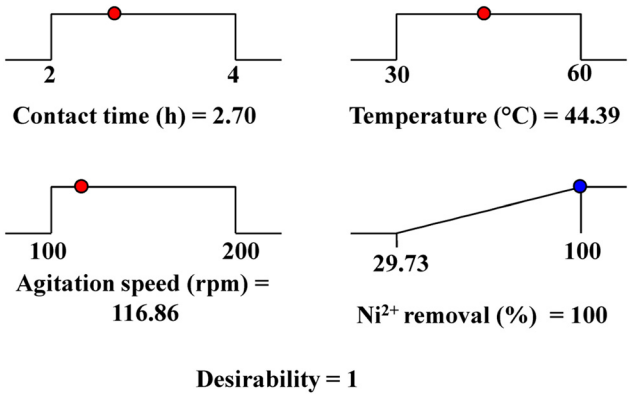

Figure 4: The optimization plot displays the DF and the optimum predicted values for the maximum percentage for biosorption of Ni^{2+} ions by *G. amansii* biomass from aqueous solution.

Zu et al. [36] reported that the biosorption of copper ions was enhanced under shaking conditions compared to static conditions using *Candida utilis* as a result of shearing power, which wrinkles the surface of yeast cells. Shaking makes conditions more available for metal uptake, as it is linked to external metal concentrations [37]. An increase in shaking velocity caused a decrease in the boundary layer resistance and increased the driving forces of diffusion of ions in the biofilm; meanwhile, the decrease in removal percentage at a higher speed was assigned to vortex formation [38].

3.7 Desirability function

The key point of the experimental design is to achieve the ideal predicted circumstances for maximizing the responses. The program's desirability function (DF) ranged from zero (undesirable) to one (desirable) for each variable. The numerical optimization detects the points at which the DF achieves the maximum Ni^{2+} biosorption percentage using the DF option in Design Expert Software. In the current study, the optimum predicted conditions were achieved using DF for the maximum simultaneous biosorption of Ni^{2+} using *G. amansii* biomass (Figure 4) with contact time, temperature, and agitation speed quantified as 2.70 h, 44.39°C, and 116.86 rpm, respectively, which achieved 100% Ni^{2+} biosorption. To confirm the biosorption percentages of Ni^{2+} by *G. amansii* biomass using the optimal predicted conditions, the experiments were conducted in triplicate, and the experimental data were compared with the predicted values. The average biosorption percentages of Ni^{2+} were also 100.0%, which revealed a high degree of correlation between the experimental and expected data. The optimization conditions for removal lead by *Turbinaria ornata* were lead concentration 99.8 $mg \cdot L^{-1}$, agitation speed 250 rpm, and adsorbent dose 16.2 $g \cdot L^{-1}$ [39].

3.8 The FTIR analysis

The FT-IR patterns of *G. amansii* biomass were recorded before and after Ni^{2+} biosorption, as illustrated in Table 6 and Figure 5, to identify the variations resulting from the interaction between the chemical functional groups on the *G. amansii* surface and Ni^{2+} ions during the biosorption process. Generally, red algal cell walls contain celluloses as well as sulfated polysaccharides such as agar

Table 6: Analysis of FTIR spectrum results of *Gelidium amansii* biomass before and after Ni^{2+} ion biosorption from aqueous solution

Before Ni^{2+} ions biosorption (A)		After Ni^{2+} ions biosorption		Difference	References
Wavenumber (cm^{-1})	Annotations	Wavenumber (cm^{-1})	Annotations		
4,414.24	O–H and C–O stretching combination band	4,413.28	O–H and C–O stretching combination band	+0.96	[40]
4,020.75	CH and C–O–C stretches and C–C vibration	4,026.54	CH and C–O–C stretches and C–C vibration	−5.79	[40]
3,960.96	Hydroxyl (OH) group	—		—	[44]
3,874.16	Hydroxyl (OH) group	—		—	[44]
3,441.12	N–H stretch	3,445.94	N–H stretch	−4.82	[47]
2,931.90	CH_2 groups	2,935.76	CH_2 groups	−3.86	[49]
1,650.16	C=O stretching	1,650.16	C=O stretching	0.0	[50]
1,538.28	C=O amide stretch	1,541.18	C=O amide stretch	−2.9	[52]
1,453.41	Stretch of C=C–C	1,443.77	Stretch of C=C–C	+9.64	[50]
1,085.96	O–H stretch	1,062.81	O–H stretch	+23.15	[53]
657.74	C–H bending vibration	658.71	C–H bending vibration	0.97	[54]
538.15	Glycosidic linkage	539.12	Glycosidic linkage	0.97	[55]

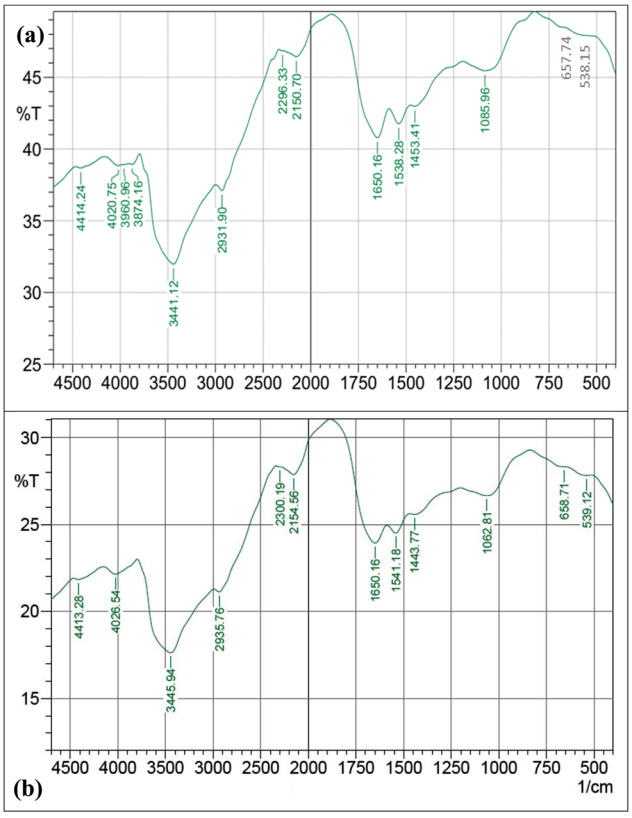

Figure 5: FTIR spectra of *Gelidium amansii* biomass: (a) before Ni^{2+} ion biosorption and (b) after Ni^{2+} ion biosorption from aqueous solution.

and carrageenan [40], the latter representing more than 75% of the dry weighted biomass [41], and carboxylic groups form the bulk acidic functional group and algal adsorption capacity are directly proportional to the existence of these active sites [19]. The weak recorded peaks at approximately 4,414.24 and 4,413.28 cm^{-1} correspond to O–H and C–O stretching combination bands, while the peaks at 4,020.75 and 4,026.54 cm^{-1} are assigned to the combination band of both CH and C–O–C stretches and C–C vibrations. All these peaks belong to cellulose [42]. Previous studies recorded that the cell walls of *G. amansii* generally contain cellulose [43]. The recorded bands between 3,400–3,900 cm^{-1} are related to hydroxyl (OH) groups, demonstrating the presence of carbohydrates [44–46], whereas galactan is a main polysaccharide in *G. amansii* [47]. The bands allocated at 3,441.12 and 3,445.94 cm^{-1} could be attributed to N–H stretches existing in aromatic amines, primary amines, and amides [48,49]. Sukwong et al. [50] reported that *G. amansii* contains proteins such as R-phycocyanin and R-phycoerythrin. The weak signals centered at approximately 2,931.90 and 2,935.76 cm^{-1} are related to CH_2 groups [51]. The obtained peaks at approximately 1,650.16 cm^{-1} exhibited C═O stretching related to carboxylic acids [52], while aromatic functions could be identified at approximately 1,538.28 and 1,541.18 cm^{-1} [53]. Pugazhendhi et al. [54] reported the appearance of a C═O amide stretch at approximately 1,500 cm^{-1}. Peaks at approximately 1,453.41 and 1,443.77 cm^{-1} displayed symmetric and asymmetric stretches of C═C–C related to aromatic rings [52]. Moreover, the FTIR peaks centered at approximately 1,085.96 and 1,062.81 cm^{-1} could be related to O–H stretching, a sign of the presence of carbohydrates and polysaccharides [52,55]. The weak resulting bands at 658.71 and 657.74 cm^{-1} can be attributed to the C–H bending vibration, which is also a sign of the presence of carbohydrates [56]. Finally, the last bending at approximately 539.13 and 538.15 cm^{-1} illustrates the presence of glycosidic linkage peaks in polysaccharides [57]. Biosorption of Ni^{2+} ions enhanced shifts of some peaks, which illustrate the interaction between different chemical functional groups of the *G. amansii* biomass surface and Ni^{2+} ions [58]. Table 7 illustrates the effects of different biosorbents related to various factors such as pH, initial Ni^{2+} ions concentrations, biomass used, temperature, and time consumed in biosorption of Ni^{2+} ions.

3.9 Scanning electron microscopy analysis

The micrograph obtained from SEM illustrated the morphological features of *G. amansii* biomass before and after the Ni^{2+} biosorption process. As exhibited in

Table 7: Effect of different biosorbent and different factors in nickel ions removal

Bio-sorbent	Initial conc. ($mg{\cdot}L^{-1}$)	pH	Biomass	Absorption	Temperature	Time	Reference
Aspergillus niger	30	6.25	2.98	70.30%	—	—	[20]
Rhodotorula glutinis	—	—	—	43%	70°C	—	[57]
Trichoderma viride	—	—	—	99.77%	—	—	[58]
Pistachio hull powder	—	—	—	14 $mg{\cdot}g^{-1}$	25 ± 3°C	1 h	[57]
Cystoseria indica	100	6	—	75%	—	20 m	[21]
Rhizopus arrhizus	100	6	—	44.2%	—	—	[22]
Acinetobacter baumannii UCR-2971	—	4.5	4.0 $g{\cdot}L^{-1}$	3.5 $mg{\cdot}g^{-1}$	—	100 m	[23]
Gelidium amansii	25	7	1 $g{\cdot}L^{-1}$	100%	44.39°C	2.7 h	This research

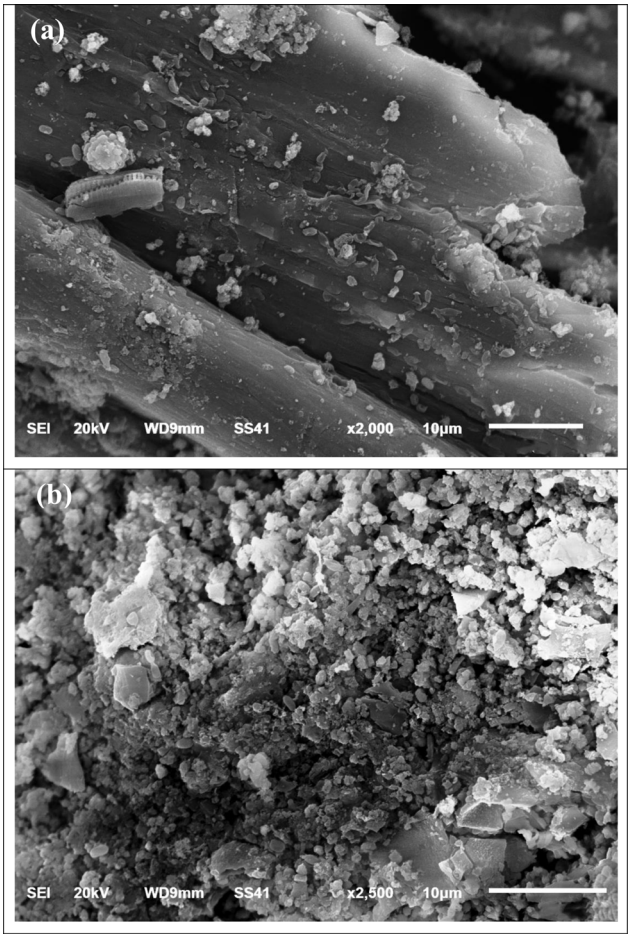

Figure 6: SEM micrograph of *G. amansii* biomass: (a) before and (b) after adsorption of Ni^{2+} ions from aqueous solution.

Figure 6a, native *G. amansii* has a plain, smooth, and uniform surface with a continuous interconnected structure, and this surface structure provides large active sites for the Ni^{2+} biosorption process. Conversely, Figure 6b demonstrates irregular, rough, and crashed surfaces accompanied by the presence of shiny spots as a result of Ni^{2+} accumulation. These variations may have resulted from vigorous cross-linking binding between negatively charged functional groups in the cell walls and positively charged Ni^{2+} [59]. The biosorption and attachment of Ni^{2+} ions on the biosorbent surface are able to perform these changes [60]. This morphological variation confirms the ability of *G. amansii* biomass to perform biosorption processes. Figure 7 shows the mechanisms of biosorption Ni^{2+} ions by *G. amansii* biomass, which demonstrates that metal ions complex with active groups in the cell wall on the cell surface in the adsorbents, and the bond formation could be covalent or electrostatic [61]. The principal binding mechanisms of the biosorption by the algae include ion exchange, formation of complex between heavy metal contaminants cations and the ligands on the algal surface, diffusion interior of the cells or surface precipitation, chelation, and bioaccumulation within the cells [62]. Red algae cell wall contains calcium carbonate beside a variety of functional groups on the surface of the algal biomass such as CH_2, C–H, C═O, N–O, C–N, –OH, PO_4, and $–NH_2$; these groups can assist adsorption sites that are responsible for metal ions biosorption [63]. There are many factors affecting heavy metals sorption mechanisms by algae. Tang et al. [64] reported that there were mutual effects between pH and heavy metal ion elimination by algae. The factor affecting the sorption mechanisms (pH, temperature, types of contaminants, and time) depends on the type of the biosorbent [65].

3.10 Electron dispersive spectroscopy analysis

EDS analysis mapping illustrates the atomic percentages of various elements for both *G. amansii* biomasses before and after adsorption of Ni^{2+} ions from the aqueous solution (Figure 8 and Tables 8 and 9). Figure 8a and Table 8 demonstrate the native *G. amansii* biomass composition

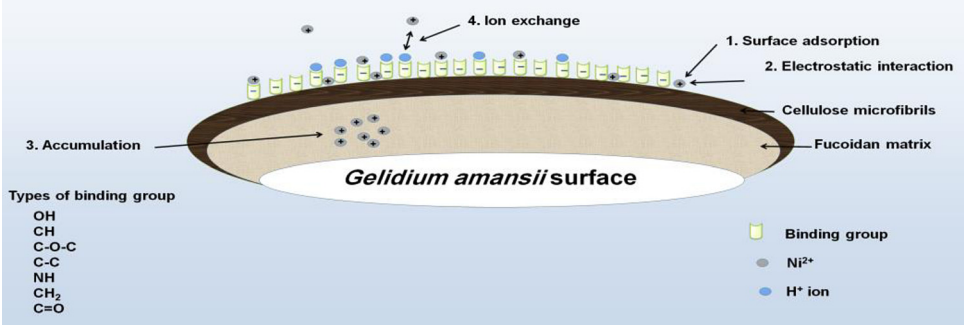

Figure 7: Mechanism of bio-removal nickel ions by *G. amansii* biomasses.

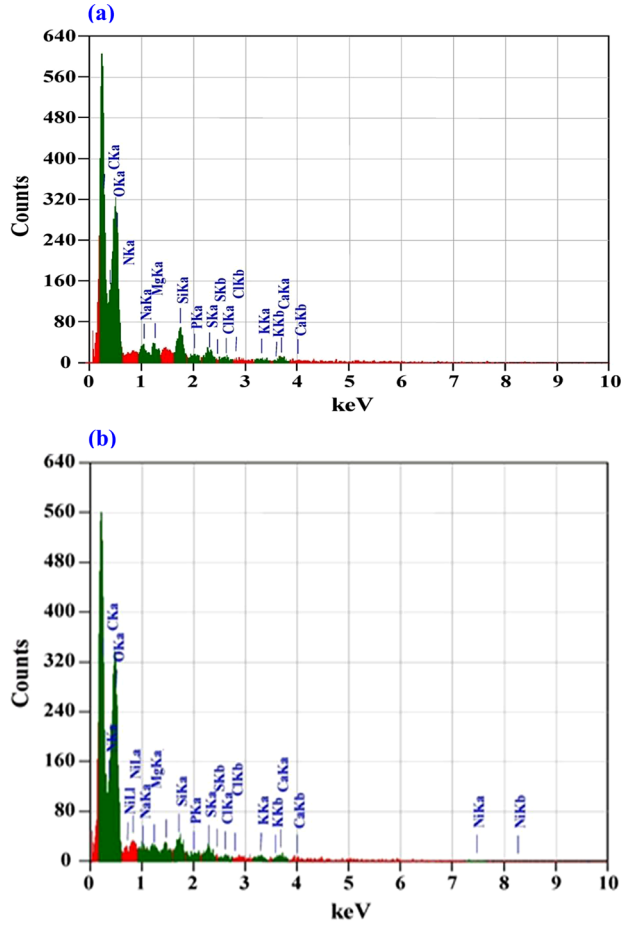

Figure 8: EDS analysis of *G. amansii* biomass: (a) before and (b) after adsorption of Ni^{2+} ions from aqueous solution. For reference, please see Tables 8 and 9.

with the dominance of carbon and oxygen with some traces of other elements, such as Na, Mg, Si, P, S, Cl, K, and Ca. Figure 8b illustrates the presence of a newly formed peak of Ni^{2+}, which confirmed the biosorption process. Overall, the algae and seaweed biomass can be used to sustainably remove heavy metals from wastewater [66].

Table 8: EDS analysis of *G. amansii* biomass before adsorption of Ni^{2+} ions from aqueous solution

Element	keV	Mass%	Error%	At%	Compound mass% cation K
C K	0.277	45.95	0.54	55.72	32.7379
O K	0.525	42.35	1.85	38.55	47.8738
Na K	1.041	1.27	1.24	0.8	1.6625
Mg K	1.253	1.17	1.03	0.7	1.4643
Si K	1.739	3.98	1.1	2.06	6.4767
P K	2.013	0.67	1.18	0.32	1.1435
S K	2.307	1.49	1.06	0.68	2.7445
Cl K	2.621	0.8	1.3	0.33	1.4863
K	3.312	0.52	1.93	0.19	0.9552
Ca K	3.69	1.8	2.36	0.56	3.4553
Total		100.00		100.00	100.00

Table 9: EDS analysis of *G. amansii* biomass after adsorption of Ni^{2+} ions from aqueous solution

Element	keV	Mass%	Error%	At%	Compound mass% cation K
C K	0.277	46	0.47	55.38	35.2614
O K	0.525	44.68	1.75	40.38	50.1642
Na K	1.041	0.27	1.26	0.17	0.3252
Mg K	1.253	0.8	1.02	0.48	0.9542
Si K	1.739	1.71	1.1	0.88	2.6077
S K	2.307	1.52	1.03	0.69	2.6697
Cl K	2.621	0.49	1.27	0.2	0.8692
K K	3.321	0.96	1.89	0.36	1.7094
Ca k	3.69	1.01	2.31	0.37	1.8648
Ni K	7.471	2.55	12.18	1.1	3.5441
Total		100.00		100.00	100.00

4 Conclusions

In the current study, *G. amansii* biomass displayed an effective capability as a sustainable biosorbent for the biosorption of Ni^{2+} from the aqueous solution. Three independent variables (contact time, temperature, and agitation–static mode) exhibited a high level of significance on the Ni^{2+} biosorption process. The maximum Ni^{2+} biosorption percentage was quantified as 100.00% under the experimental conditions of 3 h of incubation time and 45°C and 100 rpm for agitation speed. The DF confirmed optimum predicted conditions for the maximum simultaneous biosorption of Ni^{2+} using *G. amansii* biomass with contact time, temperature, and agitation speed quantified as 2.70 h, 44.39°C, and 116.86 rpm, respectively, which achieved 100% Ni^{2+} biosorption. The interaction between the *G. amansii* surface and Ni^{2+} ions during the biosorption process was illustrated using FTIR, SEM, and EDX analyses. The micrograph obtained by SEM demonstrated irregular, rough, and crashed surfaces convoyed by the occurrence of shiny spots as a result of Ni^{2+} accumulation. *G. amansii* biomass contents have dominance of carbon and oxygen with some trace elements such as Na, Mg, Si, P, S, Cl, K, and Ca as proved by EDX.

Funding information: The authors state no funding involved.

Author contributions: Noura El-Ahmady El-Naggar: provision of some necessary tools for experiments and performance the statistical design and analysis; Ragaa A. Hamouda: provision of the research topic, design of the research plan, experimental instructions, collection of the data, contribution to the interpretation of the results, and contribution substantially to the writing and revision of the manuscript; Maha M. Alharbi: provision of some necessary tools for experiments; Muhammad A. Abuelmagd: contribution to the writing of the manuscript and contribution to the interpretation of the results; Nashwa H. Rabei: provision of necessary tools for experiments and performance of the experiments; Safinaz A. Farfour: contribution to the writing of the manuscript and provision of necessary tools for experiments; Doaa Bahaa Eldin Darwish: provision of some necessary tools for experiments. All authors read and approved the final manuscript.

Conflict of interest: The authors state no conflict of interest.

Data and availability statement: The datasets spent and analyzed during this study are available from the corresponding author on reasonable request.

References

[1] Gautam PK, Gautam RK, Banerjee S, Chattopadhyaya MC, Pandey JD. Heavy metals in the environment: fate, transport, toxicity and remediation technologies. Nova Sci Publishers. 2016;60:101–30.

[2] Jia X, Fu T, Hu B, Shi Z, Zhou L, Zhu Y. Identification of the potential risk areas for soil heavy metal pollution based on the source-sink theory. J Hazard Mater. 2020;393:122424.

[3] Turhanen PA, Vepsäläinen JJ, Peräniemi S. Advanced material and approach for metal ions removal from aqueous solutions. Sci Rep. 2015;5(1):1–8.

[4] Masindi V, Muedi KL. Environmental contamination by heavy metals. Heavy Met. 2018;10:115–32.

[5] Muhammad S, Shah MT, Khan S. Health risk assessment of heavy metals and their source apportionment in drinking water of Kohistan region, northern Pakistan. Microchemical J. 2011;98:334–43.

[6] Hansul S, Fettweis A, Smolders E. De Schamphelaere K. Interactive Metal Mixture Toxicity to Daphnia magna Populations as an Emergent Property in a Dynamic Energy Budget Individual-Based Model. Environ Toxicol Chem. 2021;40:1–15. doi: 10.1002/etc.5176.

[7] Panneerselvam A, Rajadurai V, Anguraj BL. Removal of nickel from aqueous solution using synthesized IL/ZnO NPs. Environ Sci Pollut Res. 2020;27(24):29791–803.

[8] Pandey PK, Choubey S, Verma Y, Pandey M, Kamal SS, Chandrashekhar K. Biosorptive removal of Ni (II) from wastewater and industrial effluent. Int J Environ Res public health. 2007;4:332–9.

[9] Paul D. Research on heavy metal pollution of river Ganga: A review. Annals of Agrarian. Science. 2017;15(2):278–86.

[10] Borba CE, Guirardello R, Silva EA, Veit MT, Tavares CRG. Removal of nickel(II) ions from aqueous solution by biosorption in a fixed bed coloumn: Experimental and theoretical breakthrough curves. Biochemical Eng J. 2006;30:184–91.

[11] Meena AK, Mishra GK, Rai PK, Rajagopal C, Nagar PN. Removal of heavy metal ions from aqueous solutions using carbon aerogel as an adsorbent. J Hazard Mater. 2005;122(1–2):161–70.

[12] Volesky B. Advances in biosorption of metals: selection of biomass types. FEMS Microbiology Rev. 1994;14:291–302.

[13] Beni AA, Esmaeili A. Biosorption, an efficient method for removing heavy metals from industrial effluents: a review. Environ Technol & Innov. 2020;17:100503.

[14] Saha GC, Hoque MIU, Miah MAM, Holze R, Chowdhury DA, Khandaker S, et al. Biosorptive removal of lead from aqueous solutions onto Taro (Colocasiaesculenta (L.) Schott) as a low cost bioadsorbent: Characterization, equilibria, kinetics and biosorption-mechanism studies. J Environ Chem Eng. 2017;5(3):2151–62.

[15] Sanghvi AM, Martin Lo Y. Present and potential industrial applications of macro-and microalgae. Recent Pat food, Nutr & agriculture. 2010;2(3):187–94.

[16] Bilal M, Rasheed T, Sosa-Hernández JE, Raza A, Nabeel IH. Biosorption: an interplay between marine algae and potentially toxic elements-a review. Mar drugs. 2018;16(2):65.

[17] Davis TA, Volesky B, Mucci A. A review of the biochemistry of heavy metal biosorption by brown algae. Water Res. 2003;37(18):4311–30.

[18] Romera E, Gonzlez F, Ballester A, Blzquez ML, Muooz JA. Comparative study of biosorption of heavy metals using different types of algae. Bioresour Technol. 2007;98(17):3344–53.

[19] El-Naggar NE-A, Hamouda RA, Mousa IE, Abdel-Hamid MS, Rabei NH. Biosorption optimization, characterization, immobilization and application of *Gelidium amansii* biomass for complete Pb^2 removal from aqueous solutions. Sci Rep. 2018;8(1):1–19.

[20] Amini M, Younesi H, Bahramifar N. Biosorption of nickel (II) from aqueous solution by *Aspergillus niger*: Response surface methodology and isotherm study. Chemosphere. 2009;75(11):1483–91.

[21] Khajavian M, Wood DA, Hallajsani A, Majidian N. Simultaneous biosorption of nickel and cadmium by the brown algae *Cystoseria indica* characterized by isotherm and kinetic models. Appl Biol Chem. 2019;62:69. doi: 10.1186/s13765-019-0477-6.

[22] Silah H, Gül ÜD. Comparison of nickel bio-sorption properties of living and dead *Rhizopus arrhizus* bio-sorbent. AIP Conference Proceedings. Vol. 1833; 2017. p. 020105. No. 1. AIP Publishing LLC.

[23] Rodríguez CE, Quesada A. Nickel biosorption by *Acinetobacter baumannii* and *Pseudomonas aeruginosa* isolated from industrial wastewater. Braz J Microbiology. 2006;37:465–7.

[24] Montgomery DC. Design and analysis of experiments. 3rd edn. New York: Wiley; 1991.
[25] Daoud W, Ebadi T, Fahimifar A. Optimization of hexavalent chromium removal from aqueous solution using acid-modified granular activated carbon as adsorbent through response surface methodology. Korean J Chem Eng. 2015;32(6):1119–28.
[26] El-Naggar NE-A, El-Shweihy NM, El-Ewasy SM. Identification and statistical optimization of fermentation conditions for a newly isolated extracellular cholesterol oxidase-producing *Streptomyces cavourensis* strain NEAE-42. BMC Microbiol. 2016;16(1):1–20.
[27] Box GEP, Draper NR. Response surfaces, mixtures, and ridge analyses. Wiley, Canada: John Wiley & Sons; 2007.
[28] Mohamedin A, El-Naggar NE-A, Shawqi Hamza S, Sherief AA. Green synthesis, characterization and antimicrobial activities of silver nanoparticles by *Streptomyces viridodiastaticus* SSHH-1 as a living nanofactory: Statistical optimization of process variables. Curr Nanosci. 2015;11(5):640–54.
[29] Stowe RA, Mayer RP. Efficient screening of process variables. Ind Eng Chem. 1966;58(2):36–40.
[30] Gupta S, Sharma SK, Kumar A. Biosorption of Ni (II) ions from aqueous solution using modified *Aloe barbadensis* Miller leaf powder. Water Sci Eng. 2019;12(1):27–36.
[31] Nasrullah A, Khan H, Khan AS, Man Z, Muhammad N, Khan MI, et al. Potential biosorbent derived from *Calligonum polygonoides* for removal of methylene blue dye from aqueous solution. Sci World J. 2015;2015:11. doi: 10.1155/2015/562693
[32] Zafar MN, Aslam I, Nadeem R, Munir S, Rana UA, Khan SU-D. Characterization of chemically modified biosorbents from rice bran for biosorption of Ni (II). J Taiwan Inst Chem Eng. 2015;46:82–8.
[33] Liu Y-G, Ting FAN, Zeng G-m, Xin LI, Qing T, Fei YE, et al. Removal of cadmium and zinc ions from aqueous solution by living *Aspergillus niger*. Trans Nonferrous Met Soc China. 2006;16(3):681–6.
[34] Aranda-García E, Cristiani-Urbina E. Kinetic, equilibrium, and thermodynamic analyses of Ni (II) biosorption from aqueous solution by acorn shell of *Quercus crassipes*. Water Air Soil Pollut. 2018;229(4):1–17.
[35] Malamis S, Katsou E. A review on zinc and nickel adsorption on natural and modified zeolite, bentonite and vermiculite: examination of process parameters, kinetics and isotherms. J Hazard Mater. 2013;252:428–61.
[36] Zu Y-g, Zhao X-h, Hu M-S, Yuan REN, Peng X, Lei ZHU, et al. Biosorption effects of copper ions on *Candida utilis* under negative pressure cavitation. J Environ Sci. 2006;18(6):1254–9.
[37] White C, Gadd GM. The uptake and cellular distribution of zinc in *Saccharomyces cerevisiae*. Microbiology. 1987;133(3):727–37.
[38] Rajamohan NP, Kumar S, Rajasimman M, Al Qasmi F. Treatment of methanol industry effluent using algal biomass, Gelidium omanense-kinetic modeling. Chem Eng J Adv. 2021;5:100068.
[39] Abdullah Al-Dhabi N, Arasu MV. Biosorption of hazardous waste from the municipal wastewater by marine algal biomass. Env Res. 2022;204:112115.
[40] Wang J, Chen C. Biosorbents for heavy metals removal and their future. Biotechnol Adv. 2009;27(2):195–226.
[41] Yuan Y. Important chemical products from macroalgae (Ascophyllum nodosum) biorefinery by assistance of microwave technology. PhD Thesis. University of York; 2015.
[42] Invernizzi C, Rovetta T, Licchelli M, Malagodi M. Mid and near-infrared reflection spectral database of natural organic materials in the cultural heritage field. Int J Anal Chem. 2018;2018:16. doi: 10.1155/2018/7823248.
[43] Jang JH, So BR, Yeo HJ, Kang HJ, Kim MJ, Lee JJ, et al. Preparation of cellulose microfibril (CMF) from *Gelidium amansii* and feasibility of CMF as a cosmetic ingredient. Carbohydr Polym. 2021;257:117569.
[44] Kavita K, Mishra A, Jha B. Isolation and physico-chemical characterisation of extracellular polymeric substances produced by the marine bacterium Vibrio parahaemolyticus. Biofouling. 2011;27(3):309–17.
[45] Chew KW, Show PL, Yap YJ, Juan JC, Phang SM, Ling TC, et al. Sonication and grinding pre-treatments on *Gelidium amansii* seaweed for the extraction and characterization of Agarose. Front Environ Sci Eng. 2018;12(4):1–7.
[46] Mousavi SA, Almasi A, Navazeshkha F, Falahi F. Biosorption of lead from aqueous solutions by algae biomass: optimization and modeling. Desalination Water Treat. 2019;148:229–37.
[47] Kim HM, Wi SG, Jung S, Song Y, Bae H-J. Efficient approach for bioethanol production from red seaweed Gelidium amansii. Bioresour Technol. 2015;175:128–34.
[48] Devaraj P, Kumari P, Aarti C, Renganathan A. Synthesis and characterization of silver nanoparticles using cannonball leaves and their cytotoxic activity against MCF-7 cell line. J Nanotechnol. 2013;2013:5. doi: 10.1155/2013/598328.
[49] Kannan S. FT-IR and EDS analysis of the seaweeds *Sargassum wightii* (brown algae) and *Gracilaria corticata* (red algae). Int J Curr Microbiol Appl Sci. 2014;3(4):341–51.
[50] Sukwong P, Sunwoo IY, Nguyen TH, Jeong G-T, Kim S-K. R-phycoerythrin, R-phycocyanin and ABE production from *Gelidium amansii* by *Clostridium acetobutylicum*. Process Biochem. 2019;81:139–47.
[51] Guerrero P, Etxabide A, Leceta I, Peñalba M, De laCaba K. Extraction of agar from *Gelidium sesquipedale* (Rodhopyta) and surface characterization of agar based films. Carbohydr Polym. 2014;99:491–8.
[52] Sumayya SS, Murugan K. Phytochemical screening, RP-HPLC and FTIR analysis of Kappaphycus alvarezii (Doty) Doty EX PC Silva: Macro red algae. J Pharmacog Phytochem. 2017;6(1):325–30.
[53] Lee HJ, Jung SM, Lee HS, Kang S, Son JS, Jeon JH, et al. Characterization of the Photoluminescence of the Red Alga *Gelidium amansii*. Eur J Biophys. 2015;3(2):14–8.
[54] Pugazhendhi A, Prabakar D, Jacob JM, Karuppusamy I, Saratale RG. Synthesis and characterization of silver nanoparticles using *Gelidium amansii* and its antimicrobial property against various pathogenic bacteria. Microb Pathogenesis. 2018;114:41–5.
[55] Bellatmania Z, Bentiss F, Jama C, Nadri A, Reani A, Sabour B. Spectroscopic characterization and gel properties of Agar from Two *Gelidium* species from the Atlantic coast of Morocco. Biointerface Res Appl Chem. 2021;11(5):12642–52.
[56] Anand M, Suresh S. Marine seaweed *Sargassum wightii* extract as a low-cost sensitizer for ZnO photoanode based dye-sensitized solar cell. Adv Nat Sci Nanosci Nanotechnol. 2015;6(3):035008.

[57] Singh RP, Shukla MK, Mishra A, Kumari P, Reddy CRK, Jha B. Isolation and characterization of exopolysaccharides from seaweed associated bacteria *Bacillus licheniformis*. Carbohydr Polym. 2011;84(3):1019–26.
[58] Beidokhti MZ, Naeeni STO, AbdiGhahroudi MS. Biosorption of nickel (II) from aqueous solutions onto pistachio hull waste as a low-cost biosorbent. Civ Eng J. 2019;5(2):447–57.
[59] Nongmaithem N, Roy A, Bhattacharya PM. Screening of *Trichoderma* isolates for their potential of biosorption of nickel and cadmium. Braz J Microbiol. 2016;47:305–13.
[60] Fawzy M, Nasr M, Adel S, Helmi S. Regression model, artificial neural network, and cost estimation for biosorption of Ni (II)-ions from aqueous solutions by *Potamogeton pectinatus*. Int J Phytoremediat. 2018;20(4):321–9.
[61] Martini S, Afroze S. Current development of sorbents derived from plant and animal waste as green solution for treating polluted aqueous media. J Teknol. 2021;83:175–91.
[62] Hannachia Y, Dekhila A, Boubakera T. Biosorption potential of the red alga, *Gracilaria verrucosa* for the removal of Zn^{2+} ions from aqueous media: Equilibrium, kinetic and thermodynamic studies. Int J Curr Eng Technol. 2013;3:2277–4106.
[63] El-Naggar EA, Hamouda RA, El-Khateeb AY, Rabei NH. Biosorption of cationic $Hg^{2}+$ and Remazol brilliant blue anionic dye from binary solution using *Gelidium corneum* biomass. Sci Rep. 2021;11(1):1–24.
[64] Tang YZ, Gin KY, Aziz MA. The relationship between pH and heavy metal ion sorption by algal biomass. Adsorption Sci Technol. 2003;21(6):525–37.
[65] Goher ME, Abd El-Monem AM, Abdel-Satar AM, Ali MH, Hussian AE, Napiórkowska-Krzebietke A. Biosorption of some toxic metals from aqueous solution using non-living algal cells of Chlorella vulgaris. J Elementol. 2016;21(3):703–14.
[66] Znad H, Awual MR, Martini S. The utilization of Algae and seaweed biomass for bioremediation of heavy metal-contaminated wastewater. Molecules. 2022;27(4):1275.